Research on Chemical Intermediates (2019) 45:3541–3556
https://doi.org/10.1007/s11164-019-03807-2

Reduced $CuFe_2O_4$ for catalytic oxidation of methyl orange by activation of persulfate: performances and mechanisms

Qingdong Qin[1] · Jian Xu[1] · Tian Sun[1] · Yan Xu[1]

Received: 22 January 2019 / Accepted: 18 March 2019 / Published online: 28 March 2019

Abstract

Bimetallic Fe^0-based catalysts have been shown to be effective heterogeneous catalysts for elimination of organic pollutants by activating persulfate (PS). In this study, copper ferrite ($CuFe_2O_4$) was isothermally treated under a reducing atmosphere in order to load Fe^0/Cu^0 bimetallic nanoparticles on the surface of $CuFe_2O_4$. The reduced $CuFe_2O_4$ was then used as a magnetically separable catalyst for PS activation to remove methyl orange (MO) from aqueous solution. The experimental data followed well the pseudo-first-order kinetic model, and the reaction rate of the reduced $CuFe_2O_4$/PS system was 5.6 times greater than that of the $CuFe_2O_4$/PS system. The key operating parameters such as PS concentration, catalyst dosage and solution pH were investigated. Catalyst stability of reduced $CuFe_2O_4$ was also tested by consecutive reuse cycles. Quenching experiments and electron spin resonance (ESR) spectroscopy revealed that the main reactive species was sulfate radical ($SO_4^{\cdot-}$). Intermediate products of MO degradation were determined by high performance liquid chromatography coupled with a high-resolution hybrid quadrupole time-of-flight mass spectrometer (LC-Q-TOF–MS) and the MO degradation pathways were proposed. Based on the analysis of catalytic activity and surface characteristics of reduced $CuFe_2O_4$, the enhanced reactivity of reduced $CuFe_2O_4$ was mainly attributed to rapid corrosion of Fe^0/Cu^0 bimetallic nanoparticles by PS. These findings illustrated that the reduced $CuFe_2O_4$/PS system may be an efficient technology for MO removal from wastewaters.

Keywords Copper ferrite · Methyl orange · Persulfate · Sulfate radical · Catalytic oxidation

✉ Yan Xu
xuxucalmm@seu.edu.cn

[1] School of Civil Engineering, Southeast University, Nanjing 210096, China

Introduction

Water pollution caused by synthetic dyes is of great environmental concern all over the world, since most dyes are bio-recalcitrant, toxic, carcinogenic and mutagenic [1]. Thus, it is inevitable to remove dyes from wastewater before they are discharged into water resources. In recent decades, considerable attention has been paid to advanced oxidation processes (AOPs) as an efficient and versatile approach to degrade recalcitrant organic pollutants in wastewaters [2, 3]. AOPs, involving highly reactive oxygen species like hydroxyl radical (·OH), offer several advantages over conventional methods [2]. One significant advantage is the rapid transformation of recalcitrant organic compounds to biodegradable organic matter or to CO_2 and H_2O. Compared to the classic AOPs, sulfate radical ($SO_4^{\cdot-}$) related AOPs have attracted increasing research attention for decontamination of organic pollutants from water due to the fact that $SO_4^{\cdot-}$ possesses a high oxidation selectivity, strong oxidation potential (2.5–3.1 V) and wide operational pH range [4–6]. Therefore, $SO_4^{\cdot-}$ could be expected to be an excellent oxidant for the degradation of recalcitrant organic compounds in polluted water.

Generally, $SO_4^{\cdot-}$ can be generated from activating peroxymonosulfate (PMS) or persulfate (PS) by a variety of methods such as homogenous and heterogeneous metal-based catalysts, metal-free heterogeneous catalysts, heat, UV and alkaline [6–8]. Among the activation methods, heterogeneous catalysts have received more attention due to their simplicity and reusability. Moreover, PS ($0.74 per kg) is much cheaper than PMS (sold as Oxone ($2KHSO_5$–$KHSO_4$–K_2SO_4), $2.2 per kg) and even less expensive than H_2O_2 ($1.5 per kg) [9]. Thus, PS is considered to have a better application potential. Currently, metal oxides such as CuO [9], Fe_3O_4 [10], Co_3O_4 [11] and $CuFe_2O_4$ [12] have been employed as heterogeneous catalysts for PS activation. Particularly, magnetic materials are more attractive due to their easy separation from water under a magnetic field. Yet, the application of these catalysts still suffers from the low efficiency of organic pollutants removal. For example, greater than [PS]/[SMX] = 800 dose is requested to degrade sulfamethoxazole (SMX) in the Fe_3O_4/PS oxidation [10] and only 33% of diethyl phthalate is removed within 30 min in the $CuFe_2O_4$/PS oxidation [12]. Consequently, the development of efficient and magnetically recyclable heterogeneous catalysts for PS activation remains a priority.

Recently, zero-valent metal catalysts such as Fe^0 [13–15], Cu^0 [16], Zn^0 [17], Al^0 [18] and Mn^0 [19] have been investigated as PS activators. The current research trend is dominated by the Fe^0 because it is cost effective, nontoxic and more reactive [8]. Moreover, the application of Fe^0 nanoparticles as PS activator has shown an outstanding performance of organic pollutants oxidation [20]. However, due to their high surface energy, Fe^0 nanoparticles trend to aggregate, which leads to an apparent decrease in surface active sites [21]. Hence, several methods have been proposed to improve the performance of Fe^0/PS process such as coupled with ultrasound [22] and ultraviolet [23], sulfidized Fe^0 [24] and supported Fe^0 [25, 26]. Among these methods, supported Fe^0 has a great advantage because it is simple and does not need an extra energy source. Besides supported Fe^0,

bimetallic Fe^0-based catalysts are found to have significantly higher reactivity and stability compared to the single Fe^0 catalyst [27, 28]. For instance, the combination of copper with iron exhibits an improved catalytic activity due to synergic effect [27, 28]. Therefore, it is meaningful to load Fe^0/Cu^0 bimetallic nanoparticles on supports to enhance oxidation of organic pollutants by activating PS.

$CuFe_2O_4$, a kind of magnetic material, has been widely investigated in water treatment [29, 30]. It can also be used to activate PS for organic pollutants removal. However, the removal efficiency is relatively lower compared to several catalysts [12]. $CuFe_2O_4$ has both Fe and Cu elements. Therefore, to improve the catalytic activity of $CuFe_2O_4$ as PS activator, we used the hydrogen-thermal reduction method to load Fe^0/Cu^0 bimetallic nanoparticles on the surface of $CuFe_2O_4$. Then, the reduced $CuFe_2O_4$ and raw $CuFe_2O_4$ were examined as catalysts for PS activation. A common organic dye, methyl orange (MO), was selected as a model compound. The kinetics and impact factors of MO degradation were comprehensively evaluated. The catalytic mechanism for PS activation by reduced $CuFe_2O_4$ was further discussed and possible MO degradation pathways were also proposed.

Materials and methods

Reagents and materials

Unless otherwise specified, all chemicals and reagents were of reagent grade and used as received. Potassium persulfate ($K_2S_2O_8$) and MO were of analytical grade and supplied by Aladdin (China). The deionized water (DI water) with a resistivity of 18.2 MΩ cm was used in this study.

Preparation and characterization of reduced $CuFe_2O_4$

Reduced $CuFe_2O_4$ was prepared by thermal treatment of $CuFe_2O_4$ under a reducing gas atmosphere [29]. Exactly, 4.26 g $CuCl_2{\cdot}2H_2O$ and 13.52 g $FeCl_3{\cdot}6H_2O$ were added to 100 mL DI water. Then, a total of 75 mL NaOH solution (4 M) was added dropwise into the solution with continuous magnetic stirring. The solution was heated at 90 °C for 2 h. The precipitates were washed by DI water several times and dried at 70 °C overnight. Later, the precipitates were calcined at 400 °C for 4 h to obtain $CuFe_2O_4$. Finally, $CuFe_2O_4$ was treated in a H_2 stream for 4 h at 400 °C.

The morphologies of $CuFe_2O_4$ and reduced $CuFe_2O_4$ were observed by transmission electron micrograph (TEM, H-8100, Hitachi). The crystallinity was characterized by X-ray powder diffraction (XRD, PW1710, Philips) using Cu *K*α radiation. Nitrogen adsorption–desorption isotherms were measured by Micromeritics ASAP 2020 and the specific surface area (SSA) was calculated. The magnetic property (M–H curve) was measured by a vibrating sample magnetometer (VSM, Lakeshore 7407, USA). The structural information was measured by a Fourier transform spectrophotometer (FTIR, IR Affinity-1, Shimadzu) from 400 to 4000 cm^{-1} using the standard KBr disk method. The surface elemental compositions were analyzed by

X-ray photoelectron spectroscopy (XPS, Perkin-Elmer PHI-5300/ESCA, USA) with an Al *K*α X-ray source.

Catalytic degradation experiments

Batch experiments were carried out in 100 mL conical flasks in the dark to examine the catalytic degradation of catalysts. In a typical procedure, the required amount of catalyst was dispersed in 50 mg L^{-1} MO solutions with a final volume of 50 mL under vigorous magnetic stirring at 25 °C. The pH of the reaction solution was adjusted by NaOH or HCl in most of the reactions. Then, a known concentration of PS was added to the solution to initiate the reaction. Samples of 1 mL were taken out at set intervals, filtered immediately through a 0.22 μm membrane filter and quenched with excess methanol. For the investigation of reduced $CuFe_2O_4$ reusability, after each run the catalyst was filtrated, washed with DI water, dried under vacuum, and then used for the next reaction under identical experimental conditions.

Analytical methods

The concentration of MO was analyzed with a Persee T6-1610E automatic scanning UV–Vis spectrophotometer. The maximum absorbance–wavelength of MO was observed at 510 nm. The concentration of leached ions was determined by the inductively coupled plasma mass spectrometry (ICP-MS) method. Mineralization of MO was measured using a Shimadzu TOC-5000 total organic carbon (TOC) analyzer. Electron spin resonance (ESR) spectroscopy was performed by using 5,5-dimethyl-1-pyrroline-N-oxide (DMPO) as trapping agent to examine reactive oxygen species produced in the heterogeneous reaction. The intermediates of MO degradation were detected using high performance liquid chromatography (HPLC; Agilent Technologies, Waldbronn, Germany) coupled with a high-resolution hybrid quadrupole time-of-flight mass spectrometer (Triple TOF 5600, AB Sciex, Foster City, CA) with an electrospray ionization (ESI) source operating in positive and negative ion modes (LC-Q-TOF–MS). A BEH C18 column (2.1 mm × 50 mm, 2.5 μm, Waters, USA) was used to separate chemicals. The mobile phases used were 2 mM ammonium acetate in 5% methanol aqueous solution (A) and methanol (B).

Results and discussion

Characterization of reduced $CuFe_2O_4$

The TEM images (Fig. 1a) showed the surface morphologies of $CuFe_2O_4$ and reduced $CuFe_2O_4$. It was obvious that the surface of the $CuFe_2O_4$ was relatively smooth. Meanwhile, the surface of the reduced $CuFe_2O_4$ was relatively rough and composed of many nanoparticles, implying that Fe^0/Cu^0 bimetallic nanoparticles were well loaded onto the surface of $CuFe_2O_4$. XRD patterns of the synthesized samples are presented in Fig. 1b. The XRD patterns illustrated that the $CuFe_2O_4$

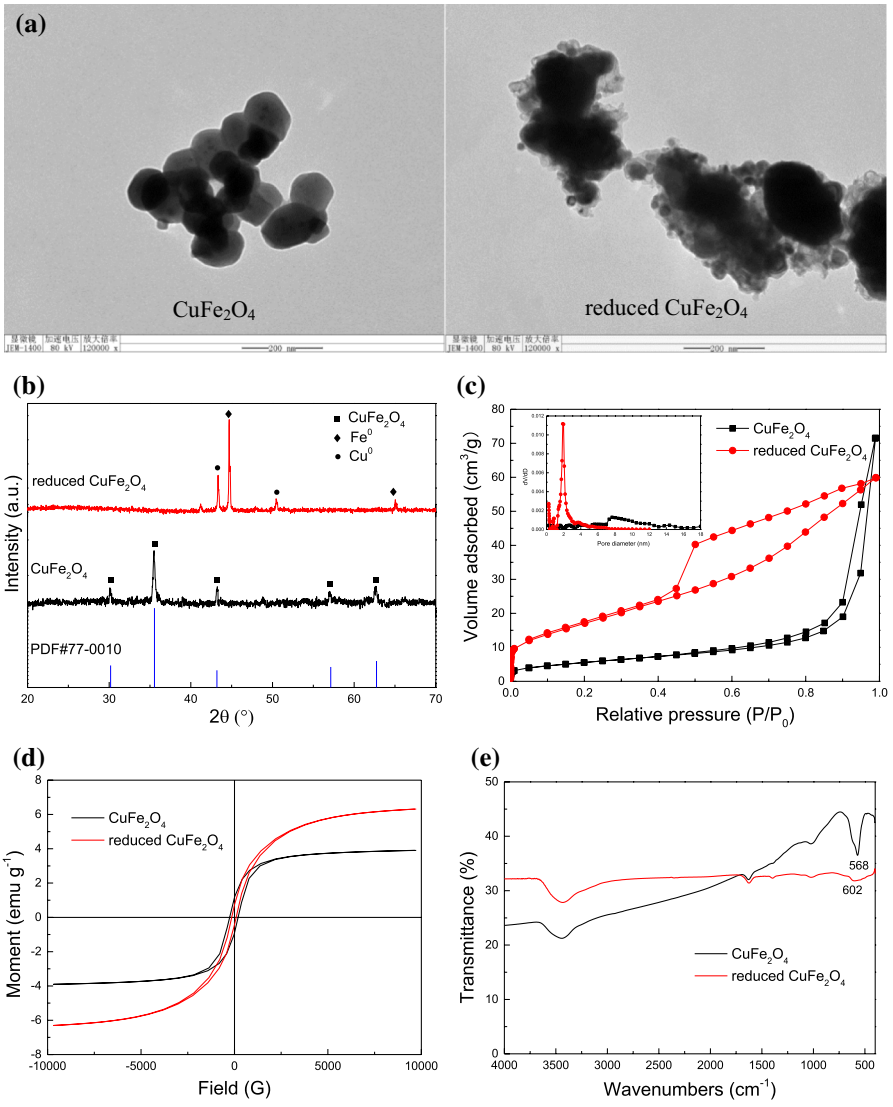

Fig. 1 The TEM images (**a**), XRD patterns (**b**), N_2 adsorption/desorption isotherms and pore size distributions (**c**), magnetization curves (**d**) and FTIR spectra (**e**) of $CuFe_2O_4$ and reduced $CuFe_2O_4$

was highly crystallized, which was in agreement with PDF #77-0010. In the pattern of the reduced $CuFe_2O_4$, two characteristic peaks for Fe^0 (PDF #99-0064) and two characteristic peaks for Cu^0 (PDF #70-3039) were observed simultaneously, indicating the formation of Fe^0 and Cu^0 on the $CuFe_2O_4$ surface. The SSA of $CuFe_2O_4$ and reduced $CuFe_2O_4$ was obtained from the N_2 physisorption isotherms (Fig. 1c). $CuFe_2O_4$ and reduced $CuFe_2O_4$ had the SSA of 15.6 and 51.8 $m^2\ g^{-1}$, respectively. The relatively higher SSA of the reduced $CuFe_2O_4$ tended to provide

abundant active sites for PS activation. The pore size distribution of 2–8 nm guaranteed efficient transportation of pollutants to the reduced $CuFe_2O_4$. The magnetization curve of reduced $CuFe_2O_4$ showed a typical superparamagnetic S-like curve with the saturated magnetization of 6.3 emu g^{-1}, indicating the magnetic property of reduced $CuFe_2O_4$ (Fig. 1d). Meanwhile, the specific saturation magnetization value of reduced $CuFe_2O_4$ was higher than that of $CuFe_2O_4$. This is because the higher amount of iron in reduced $CuFe_2O_4$, which will give rise to a high magnetization value [31]. The FTIR spectra of $CuFe_2O_4$ and reduced $CuFe_2O_4$ are presented in Fig. 1e. For the $CuFe_2O_4$, the peak at 568 cm^{-1} was assigned to the symmetric stretching vibration of the Fe–O band in the tetrahedral FeO_6 groups of spinel-type compounds [32]. After reduction, a remarkable shift to 602 cm^{-1} was observed, suggesting the change of $CuFe_2O_4$ surface structure.

Catalytic activity of reduced $CuFe_2O_4$

MO removal efficency in the presence of PS, reduced $CuFe_2O_4$, PS + $CuFe_2O_4$ and PS + reduced $CuFe_2O_4$ was examinated, respectively. As shown in Fig. 2a, greater than 72.5% of MO was removed in the reduced $CuFe_2O_4$/PS system after 30 min reaction, whereas only 28.4% of MO was removed in the $CuFe_2O_4$/PS system, which demonstrated a significant enhancement of catalytic activity of $CuFe_2O_4$ by use of H_2 reduction. Moreover, no remarkable degradation of MO was observed in the presence of PS and the adsorption of MO by reduced $CuFe_2O_4$ was less than 16%. These findings clearly indicated that the removal of MO in the reduced $CuFe_2O_4$/PS system was most likely due to the activation of PS by reduced $CuFe_2O_4$. The remaining TOC in solution was also measured after 30 min of reaction in the reduced $CuFe_2O_4$/PS system. The TOC was removed less than 5% in 30 min. The relatively low TOC removal efficiency is probably due to the low PS dose and the short reaction time [14, 28].

It has been reported that the heterogeneous activation of PS is controlled by both the catalyst surface structure and composition [33]. The higher SSA will provide

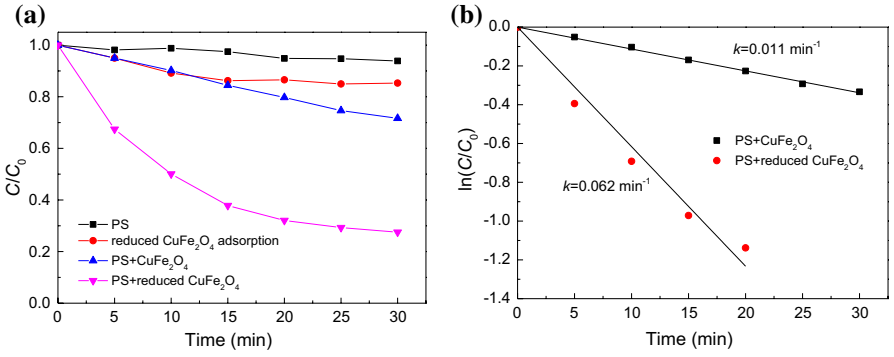

Fig. 2 Comparison of the removal efficiency of MO with different catalytic systems (**a**) and plot of $\ln(C/C_0)$ versus reaction time (**b**). Conditions: $[PS]_0 = 1$ mM, catalyst dosage = 0.1 g L^{-1}, $[MO]_0 = 50$ mg L^{-1}, initial pH = 3.2 ± 0.1

more active sites, which is expected to accelerate the reactions of PS decomposition. Therefore, to better evaluate the catalytic reactivity, the reaction rates were normalized by SSA. Here, the pseudo-first-order kinetic model ($C = C_0\exp(-kt)$) was used to describe the concentration profile of MO degradaion (Fig. 2b). The reaction rate k (min^{-1}) of $CuFe_2O_4$ and reduced $CuFe_2O_4$ was calculated to be 0.011 ($R^2 = 0.999$) and 0.062 ($R^2 = 0.989$) min^{-1}, respectively. After normalization, the constant for the reduced $CuFe_2O_4$ (1.20×10^{-3} g m^{-2} min^{-1}) was more than 1.7 times higher than that for $CuFe_2O_4$ (0.71×10^{-3} g m^{-2} min^{-1}), indicating the active sites on the reduced $CuFe_2O_4$ surface were more reactive. It also suggested that Fe^0 and Cu^0 bimetallic particles in the reduced $CuFe_2O_4$ surface played important roles for effective PS activation.

In general, the PS activation mechanism by Fe^0 involves a slow-releasing of dissolved Fe^{2+} from Fe^0 through corrosion (Eq. 1) [13]. Fe^{2+} then activates PS through electron transfer to produce $SO_4^{\cdot-}$ (Eq. 2) [13, 14]. Similarly, Cu^0 corrodes to form dissolved Cu^+ in the presence of PS (Eq. 3) [16]. Thereafter, Cu^+ activates PS via one-electron transfer to generate $SO_4^{\cdot-}$ (Eq. 4).

$$Fe^0 + S_2O_8^{2-} \rightarrow Fe^{2+} + 2SO_4^{2-} \quad (1)$$

$$Fe^{2+} + S_2O_8^{2-} \rightarrow Fe^{3+} + SO_4^{2-} + SO_4^{\cdot-} \quad (2)$$

$$2Cu^0 + S_2O_8^{2-} \rightarrow 2Cu^+ + 2SO_4^{2-} \quad (3)$$

$$Cu^+ + S_2O_8^{2-} \rightarrow Cu^{2+} + SO_4^{2-} + SO_4^{\cdot-} \quad (4)$$

Hence, the in situ generation of total dissolved metal ions in the reduced $CuFe_2O_4$/PS system was measured. As shown in Fig. 3, the amount of soluble iron and copper ions gradually increased as reaction time increased. The concentrations of iron and copper ions were 36.9 and 6.6 mg L^{-1} after 30 min reaction, respectively. In order to

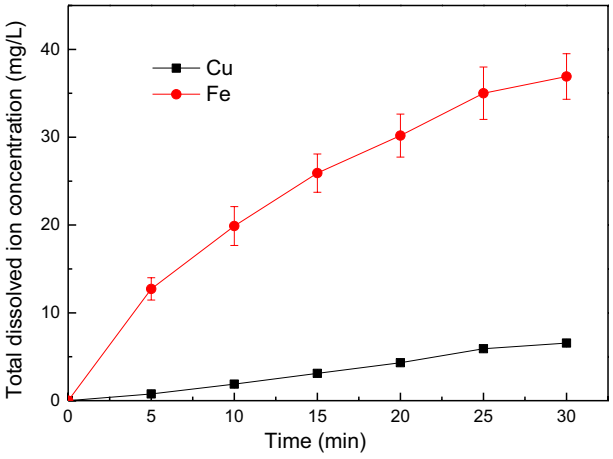

Fig. 3 Total dissolved metal ions in the system. Conditions: $[PS]_0 = 1$ mM, catalyst dosage = 0.1 g L^{-1}, $[MO]_0 = 50$ mg L^{-1}, initial pH = 3.2 ± 0.1

confirm the formation of metal ions associated with PS reaction, the leached metal ions were also measured without PS addition. The results showed that the leached iron and copper ions were 0.37 and 1.1 mg L^{-1} after 30 min reaction, respectively, which were much lower than addition of PS. This observation revealed that PS accelerated the corrosion of Fe^0 and Cu^0 to release metal ions during the reduced $CuFe_2O_4$/PS oxidation process (Eqs. 1–4).

Effects of parameters on MO degradation

Figure 4a illustrates the effect of PS concentration on the removal of MO using reduced $CuFe_2O_4$. It was clearly observed that the removal of MO increased while increasing the PS concentration. The higher the PS concentration, the faster the degradation rate that was obtained. The reaction rate increased from 0.041 to 0.112 min^{-1} when PS increased from 0.5 to 2.0 mM. This was likely that the generation of highly reactive oxygen species ($SO_4^{\cdot-}$ and/or ·OH) would increase along with the increase in PS initial concentration, leading to a high MO degradation rate.

Figure 4b shows the effect of reduced $CuFe_2O_4$ dose on MO degradation. It can be seen that the removal of MO increased with the increase in reduced $CuFe_2O_4$ dose due to the availability of more active sites. However, when its dose increased from 0.1 to 0.2 g L^{-1}, a slight decline in the final degradation after 30 min reaction was noticed. This decline was probably due to the scavenging effect of Fe(II) [6]. At a high catalyst dose, a large amount of Fe(II) will form, which will scavenge $SO_4^{\cdot-}$ through undesirable reactions (Eq. 5). In addition, excessive amounts of $SO_4^{\cdot-}$ will be generated at an excess addition of catalyst. Then, $SO_4^{\cdot-}$ will disappear by the combination between $SO_4^{\cdot-}$ themselves (Eq. 6). Similar phenomena were also found in other studies with a high catalyst dose [26, 34, 35].

$$Fe^{2+} + SO_4^{\cdot-} \rightarrow Fe^{3+} + SO_4^{2-} \quad (5)$$

$$SO_4^{\cdot-} + SO_4^{\cdot-} \rightarrow S_2O_8^{2-} \quad (6)$$

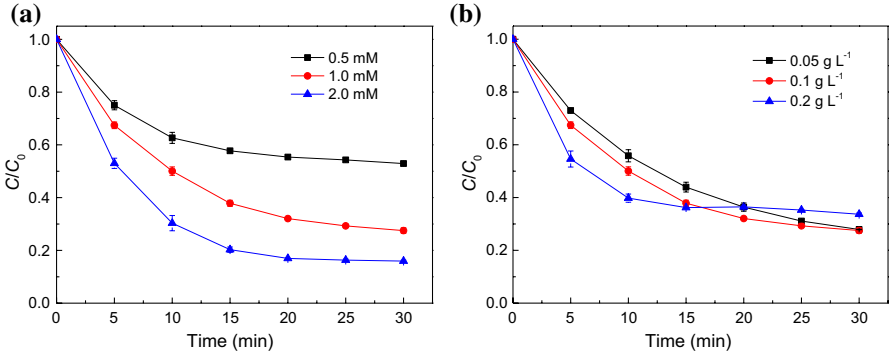

Fig. 4 Effect of PS concentration (**a**) and catalyst dose (**b**) on MO degradation by reduced $CuFe_2O_4$. Conditions: Catalyst dosage = 0.1 g L^{-1} for (**a**), $[PS]_0$ = 1 mM for (**b**), $[MO]_0$ = 50 mg L^{-1}, initial pH = 3.2 ± 0.1

Figure 5 shows the effect of initial pH on the removal of MO by reduced $CuFe_2O_4$/PS oxidation. It can be seen that the degradation of MO was significantly influenced by solution pH. The degradation of MO decreased with the increased pH of the solution. The degradation of MO was 72.5%, 56.0%, 41.0% and 22.5% at pH 3.2, 5.6, 7.1 and 9.2 after 30 min, indicating it more favorable for the degradation of MO at acidic pH. The relatively slow degradation of MO at higher pH values may be attributed to a repulsive force prevailing between the $S_2O_8^{2-}$ and the negatively charged surface of reduced $CuFe_2O_4$. The pH of the point of zero charge (pH_{PZC}) of reduced $CuFe_2O_4$ was assumed to be less than 8.0 since the pH_{PZC} of Fe^0, Cu^0 and $CuFe_2O_4$ was 7.8 [36], 5.17 [16] and 7.9 [30], respectively. Thus, the reduced $CuFe_2O_4$ surface has a negative charge at pH higher than its pH_{PZC}. The repulsive force between the reduced $CuFe_2O_4$ surface and $S_2O_8^{2-}$ would inhibit $S_2O_8^{2-}$ to reach the catalyst surface and accelerate the electron transfer [37]. Moreover, metal ions will form precipitates at higher pH, and the precipitates can not provide new active sites [38]. On the other hand, as Fe^0 and Cu^0 were loaded onto the surface of reduced $CuFe_2O_4$, the lower pH will favor the generation of Fe^{2+} and Cu^+ (Eqs. 7, 8), which could promote the decomposition of PS into $SO_4^{\cdot-}$ [16, 39]. Similar degradation profiles were also observed by other researchers using Fe^0 or Cu^0 as PS activator to degrade organic compounds [15, 16, 38, 39].

$$Fe^0 + 2H^+ \rightarrow Fe^{2+} + H_2 \tag{7}$$

$$Cu^0 + 2H^+ \rightarrow Cu^+ + H_2 \tag{8}$$

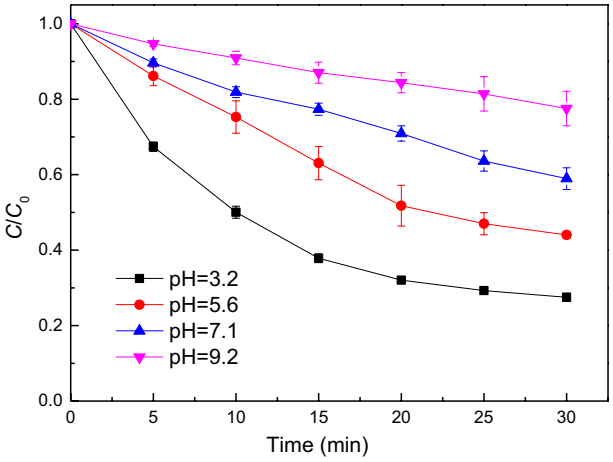

Fig. 5 Effect of pH on MO degradation by reduced $CuFe_2O_4$. Conditions: $[PS]_0 = 1$ mM, catalyst dosage = 0.1 g L^{-1}, $[MO]_0 = 50$ mg L^{-1}

Reusability of reduced $CuFe_2O_4$

For stability evaluation of the catalyst, the reduced $CuFe_2O_4$ was collected after the degradation reaction, washed with DI water and dried under vacuum. Figure 6 shows the degradation of MO for three consecutive runs. As observed, the removal of MO gradually decreased during three runs. The overall removals of MO after 30 min at each run were 72.5%, 68.9% and 58.1%, respectively. The main reason for this decrease can be attributed to the active constituent leaching from catalyst and/or catalyst poisoning caused by intermediates. The total concentration of metal ions remained in the solution was detected to be greater than 30 mg L^{-1} at each 30 min reaction, which suggested the loss of catalyst activity was mainly caused by metal leaching. Further studies are still required to diminish the leaching of active components from the catalyst. The XRD patterns of the reduced $CuFe_2O_4$ before and after reaction are presented in Fig. 7. The crystal phase of the used catalyst was almost the same as that of the fresh catalyst, indicating that no new product was generated. Ji et al. [27] also have found the similar result that no new peak was observed in XRD spectrum of the Fe^0/Cu^0-PS system. Overall, reduced $CuFe_2O_4$ exhibited a fairly good PS activation efficiency for reuse in several runs without any significant drop in catalytic activity.

The reaction mechanism

In order to investigate the major reactive species responsible for MO degradation, classical quenching tests using ethanol and *tert*-butyl alcohol (TBA) as quenching agents were carried out [40]. Ethanol and TBA are usually used to differentiate $SO_4^{\cdot-}$ from ·OH as the reaction rates of TBA with $SO_4^{\cdot-}$ and ·OH are distinguishable. The effects of ethanol and TBA on reduced $CuFe_2O_4$/PS oxidation are shown in Fig. 8.

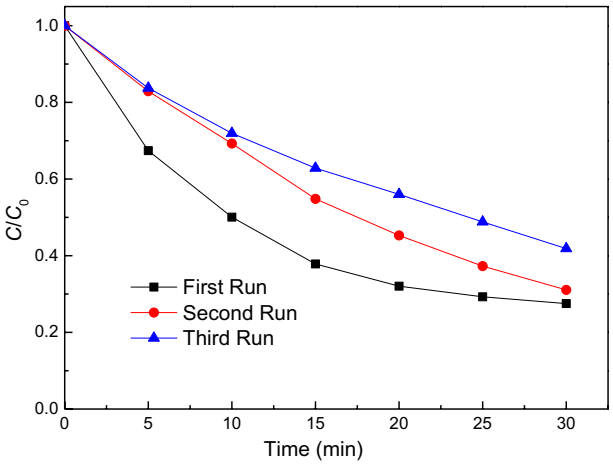

Fig. 6 Degradation of MO by reduced $CuFe_2O_4$/PS in three successive runs. Conditions: $[PS]_0 = 1$ mM, catalyst dosage = 0.1 g L^{-1}, $[MO]_0 = 50$ mg L^{-1}, initial pH = 3.2 ± 0.1

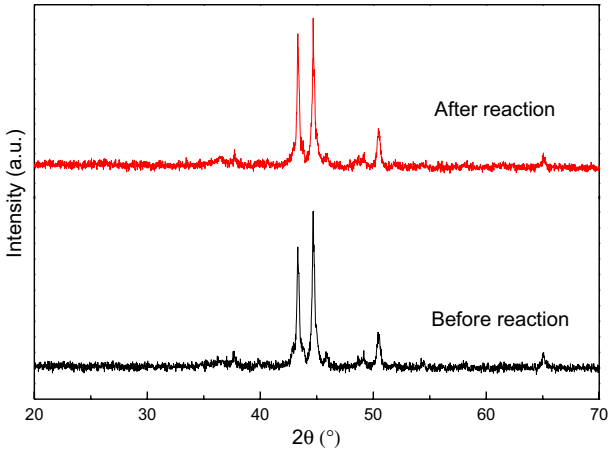

Fig. 7 XRD patterns of reduced $CuFe_2O_4$ before and after reaction

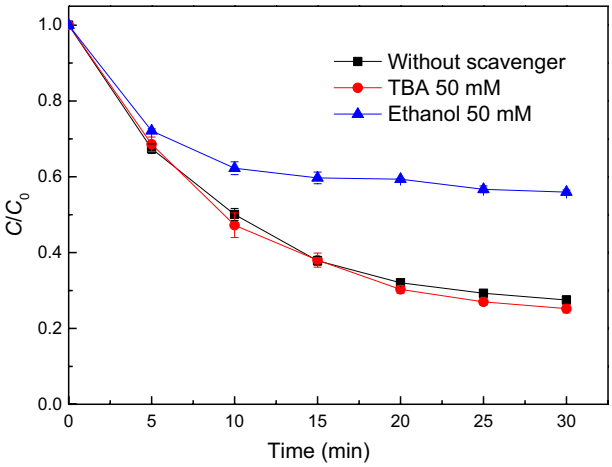

Fig. 8 Effect of TBA and ethanol on MO degradation by reduced $CuFe_2O_4$. Conditions: $[PS]_0 = 1$ mM, catalyst dosage = 0.1 g L^{-1}, $[MO]_0 = 50$ mg L^{-1}, initial pH = 3.2 ± 0.1

It can be seen that ethanol had a much higher inhibition effect on the degradation of MO compared with TBA. When TBA was added, no significant decrease in MO degradation was observed, suggesting that ·OH was subsequently ruled out in this system. However, when 50 mM ethanol was added in the original reaction solution, the removal of MO was significantly inhibited. Therefore, the dominant reactive species for MO degradation were suggested to be $SO_4^{\cdot-}$ based on the quenching experiments.

To further confirm the major reactive species, ESR experiments were conducted to monitor the types of radicals generated during the degradation of MO.

As shown in Fig. 9, the signals of DMPO radical adducts in the reduced $CuFe_2O_4$ catalyzed PS system were much stronger than the pure PS system, indicating that the generation of radicals was significantly facilitated by the addition of reduced $CuFe_2O_4$ into the PS system. Furthermore, signals of both ·OH and $SO_4^{\cdot-}$ radicals were observed in the reduced $CuFe_2O_4$ catalyzed PS system. It has been well reported in many studies that Fe^0 and Cu^0 mainly activated PS to generate $SO_4^{\cdot-}$ [8, 13, 16, 26]. In addition, the dominant reactive species for MO degradation were $SO_4^{\cdot-}$ based on quenching experiments in this study. Therefore, the observed strong signals of DMPO-OH adducts were possibly attributed to the fast transformation from DMPO-SO_4 to DMPO-OH via nucleophilic substitution [41]. These phenomena were also observed in Fe^0/PS and Co_3O_4/PS systems [11, 42].

Previous studies suggested that PS can be activated by Fe^0 and Cu^0 to produce $SO_4^{\cdot-}$ via Eqs. (1)–(4) [13, 14, 16]. The leached metal ions result in this study revealed that PS could accelerate the corrosion of Fe^0 and Cu^0 to release metal ions. Therefore, the surface characteristics of reduced $CuFe_2O_4$ may be changed during reaction. Then, XPS technique was used to characterize the chemical compositions of reduced $CuFe_2O_4$ after reaction. As shown in Fig. 10a, the binding energy at 710.2 and 712.3 eV can be assigned to Fe(II) and Fe(III), respectively. After reaction, the peak at 706.1 eV assigned to Fe^0 disappeared, and the percentage of Fe(III) increased from 18.0 to 52.3%, suggesting the oxidation of Fe(II) to Fe(III) via reacting with PS. Wu et al. [26] proposed that Fe^0 could react with $S_2O_8^{2-}$ to generate Fe(II), which activated PS to yield $SO_4^{\cdot-}$ and conduced to the oxidation of atrazine. As shown in Fig. 10b, the atomic ratio of Cu^0 decreased from 10.6 to 6.8% after reaction, suggesting the reaction of Cu^0 in aqueous solution. Zhou et al. [16] concluded that Cu^0 could react with H^+ in acidic conditions to produce Cu^+, and the presence of PS also could strongly enhance the corrosion and Cu^+ release. Then, the generated Cu^+ further decomposed PS to

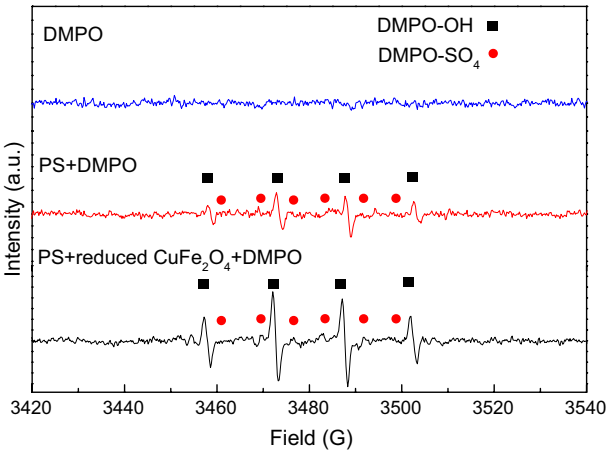

Fig. 9 DMPO spin trapping ESR spectra in the systems

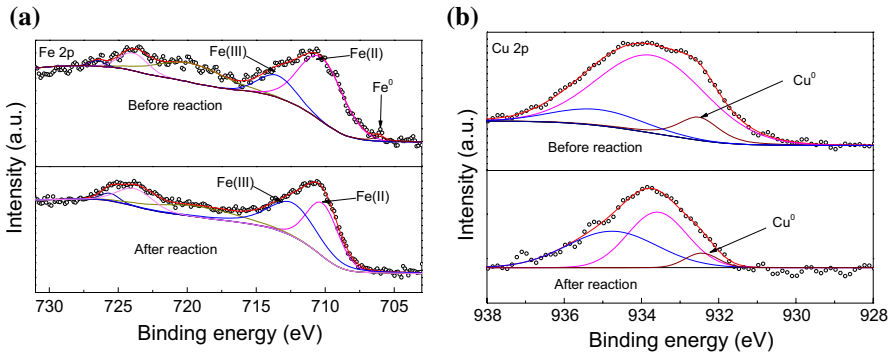

Fig. 10 XPS spectra for Fe 2*p* (**a**) and Cu 2*p* (**b**) of reduced $CuFe_2O_4$ before and after reaction

produce $SO_4^{\cdot-}$. Accordingly, a possible mechanism of MO degradation by reduced $CuFe_2O_4$ was proposed as illustrated in Fig. 11.

Degradation pathways

Usually, $SO_4^{\cdot-}$ oxidation of aromatic compounds in the first step includes: (1) single electron transfer; (2) hydrogen atom abstraction; and (3) radical adduct formation [43]. To investigate the degradation pathway of MO, LC-Q-TOF–MS was used to identify the intermediates including protonated ion ($[M+H]^+$). As shown in Fig. 12, five products were tentatively identified. The intermediate products included 4-[(4-methyl amino) phenyl diazenyl] benzene sulphonate (*m*/*z* 290), 4-hydroxybenzenesulfonic acid (*m*/*z* 173), benzenesulfonic acid (*m*/*z* 157), 2-*N*,*N*-dimethyl aniline diazine (*m*/*z* 150) and *N*-methyl aniline diazine (*m*/*z* 136). According to the chemical structures of the identified oxidation intermediates, pathways for the degradation of MO were postulated (Fig. 13). The degradation was primarily achieved by attack of $SO_4^{\cdot-}$ on MO. The compound with *m*/*z* 290 was formed by demethylation of MO, which further underwent breaking of the –C–N– bond. Demethylation of MO by attack of $SO_4^{\cdot-}$ was also observed in the copper nanoparticles/PMS system [44]. Compounds with *m*/*z*

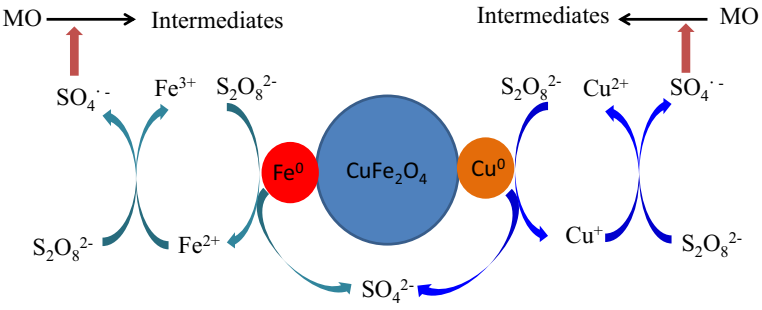

Fig. 11 Schematic diagram of MO degradation mechanism by reduced $CuFe_2O_4$

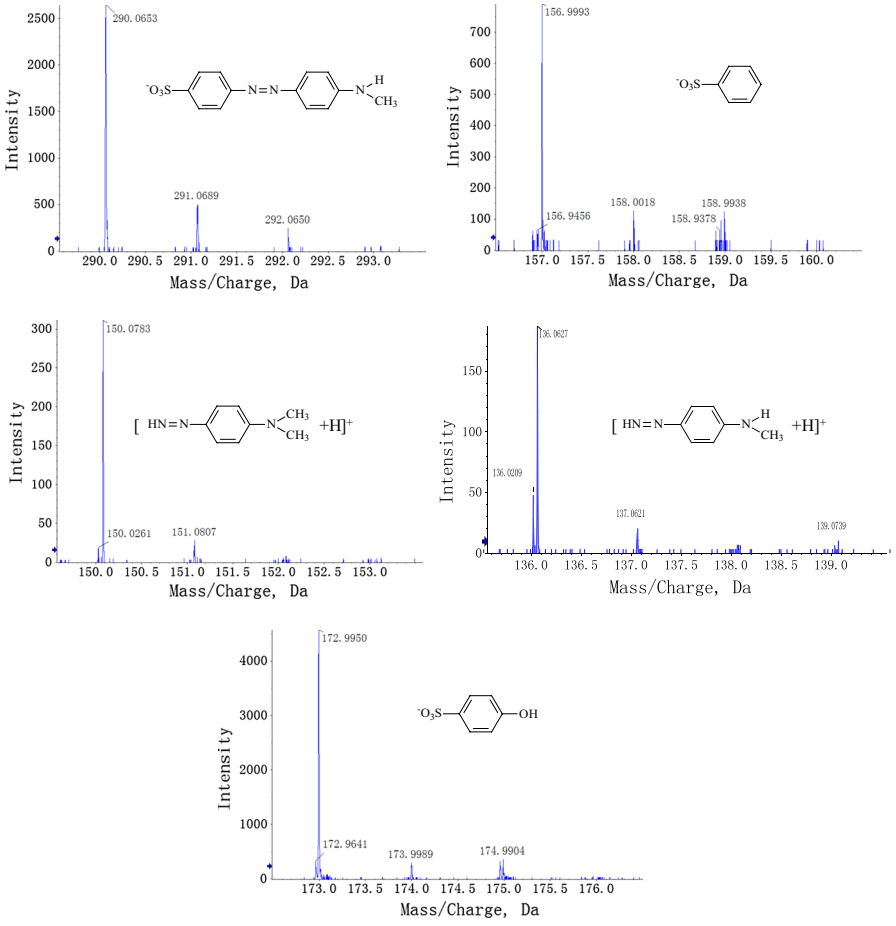

Fig. 12 Proposed structures and TOF–MS spectra of the MO degradation products

157 and 150 were formed by cleavage of the –C–N– bond near the azo bond in MO. The compound with *m*/*z* 136 was derived from the compound with *m*/*z* 290 after azo bond cleavage. Moreover, the compound with *m*/*z* 173 was another transformation pathway of the MO transformation. First, $SO_4^{\cdot-}$ attacked the compounds (*m*/*z* 304 and *m*/*z* 290), producing a radical cation at the carbon center. Then, subsequent addition of H_2O led to the production of 4-hydroxybenzenesulfonic acid. This intermediate has been also observed in oxidation of Acid Orange 7 by reaction with $SO_4^{\cdot-}$ [45]. Overall, these identified intermediates clearly indicated that MO degradation mainly underwent $SO_4^{\cdot-}$ oxidation.

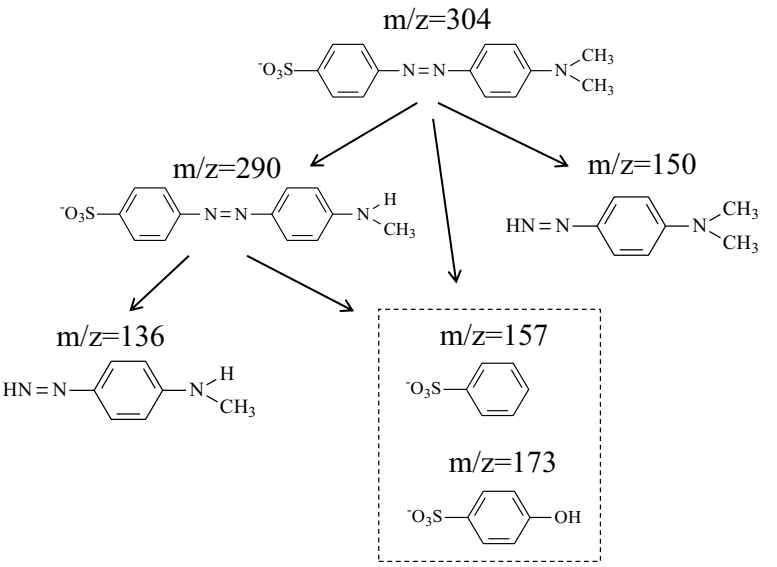

Fig. 13 Proposed oxidative degradation route of MO in reduced $CuFe_2O_4$/PS system

Conclusions

Reduced $CuFe_2O_4$ showed a superior activity in PS activation for degradation of MO in water compared with raw $CuFe_2O_4$. The presence of Fe^0 and Cu^0 nanoparticles on the surface of reduced $CuFe_2O_4$ was proved to play an important role in the high catalytic activity. The catalyst stability tests revealed that reduced $CuFe_2O_4$ possessed a relatively good PS activation efficiency for reuse in several runs. The quenching experiments and ESR measurements verified that $SO_4^{\cdot-}$ was the major radical species to degrade MO in reduced $CuFe_2O_4$/PS oxidation. On the basis of XPS and LC-Q-TOF–MS results, the mechanisms and pathways were proposed for MO degradation. Although the catalytic and magnetic properties of reduced $CuFe_2O_4$ show a potential availability in wastewater treatment, further work is needed to diminish the leaching of active components from the catalyst.

Acknowledgements This work was supported by the National Natural Science Foundation of China [41671468 and 51408119], Fundamental Research Funds for the Central Universities and State Key Laboratory of Pollution Control and Resource Reuse (PCRRF16020). The authors would like to thank the Analytical Center of NIGLAS for making this study possible by making laboratory facilities available. The authors are grateful to Dr. Nanyang Yu and Dr. Si Wei at Nanjing University for providing the LC-Q-TOF–MS method.

Compliance with ethical standards

Conflict of interest There are no conflicts of interest to declare.

References

1. P. Verma, S.K. Samanta, Environ. Chem. Lett. **16**, 969 (2018)
2. J.L. Wang, L.J. Xu, Crit. Rev. Environ. Sci. Technol. **42**, 251 (2012)
3. O. Acisli, A. Khataee, R.D.C. Soltani, S. Karaca, Ultrason. Sonochem. **35**, 210 (2017)
4. P.D. Hu, M.C. Long, Appl. Catal. B Environ. **181**, 103 (2016)
5. F. Ghanbari, M. Moradi, Chem. Eng. J. **310**, 41 (2017)
6. I.A. Ike, K.G. Linden, J.D. Orbell, M. Duke, Chem. Eng. J. **338**, 651 (2018)
7. J.L. Wang, S.Z. Wang, Chem. Eng. J. **334**, 1502 (2018)
8. W.D. Oh, T.T. Lim, Chem. Eng. J. **358**, 110 (2019)
9. T. Zhang, Y. Chen, Y.R. Wang, J. Le Roux, Y. Yang, J.P. Croue, Environ. Sci. Technol. **48**, 5868 (2014)
10. Y.L. Wu, Y.H. Shi, H.C. Chen, J.F. Zhao, W.B. Dong, Process Saf. Environ. Protect. **116**, 468 (2018)
11. J. Zhang, M.Y. Chen, L. Zhu, RSC Adv. **6**, 758 (2016)
12. X.L. Zhang, M.B. Feng, R.J. Qu, H. Liu, L.S. Wang, Z.Y. Wang, Chem. Eng. J. **301**, 1 (2016)
13. C. Kim, J.Y. Ahn, T.Y. Kim, W.S. Shin, I. Hwang, Environ. Sci. Technol. **52**, 3625 (2018)
14. S.Y. Oh, S.G. Kang, P.C. Chiu, Sci. Total Environ. **408**, 3464 (2010)
15. C.A.L. Graca, L.T.N. Fugita, A.C. de Velosa, A. Teixeira, Environ. Sci. Pollut. Res. **25**, 5474 (2018)
16. P. Zhou, J. Zhang, Y.L. Zhang, G.C. Zhang, W.S. Li, C.M. Wei, J. Liang, Y. Liu, S.H. Shu, J. Hazard. Mater. **344**, 1209 (2018)
17. C. Chen, Y.J. Han, J. Guo, L.X. Zhou, Y.Q. Lan, J. Taiwan Inst. Chem. Eng. **88**, 169 (2018)
18. T.F. Ren, S.Y. Yang, Y.T. Jiang, X.R. Sun, Y.X. Zhang, Chem. Eng. J. **348**, 350 (2018)
19. N.S. Shah, J.A. Khan, M. Sayed, Z.U. Khan, H.S. Ali, B. Murtaza, H.M. Khan, M. Imran, N. Muhammad, Chem. Eng. J. **356**, 199 (2019)
20. H.X. Li, J.Q. Wan, Y.W. Ma, Y. Wang, M.Z. Huang, Chem. Eng. J. **237**, 487 (2014)
21. R. Sharma, S. Bansal, S. Singhal, RSC Adv. **5**, 6006 (2015)
22. T. Zhou, X.L. Zou, J. Mao, X.H. Wu, Appl. Catal. B Environ. **185**, 31 (2016)
23. Y.W. Pan, Y. Zhang, M.H. Zhou, J.J. Cai, Y.S. Tian, Chem. Eng. J. **361**, 908 (2019)
24. M.P. Rayaroth, C.S. Lee, U.K. Aravind, C.T. Aravindakumar, Y.S. Chang, Chem. Eng. J. **315**, 426 (2017)
25. M.B. Gu, U. Farooq, S.G. Lu, X. Zhang, Z.F. Qiu, Q. Sui, J. Hazard. Mater. **349**, 35 (2018)
26. S.H. Wu, H.J. He, X. Li, C.P. Yang, G.M. Zeng, B. Wu, S.Y. He, L. Lu, Chem. Eng. J. **341**, 126 (2018)
27. Q.Q. Ji, J. Li, Z.K. Xiong, B. Lai, Chemosphere **172**, 10 (2017)
28. C.X. Wang, J.Q. Wan, Y.W. Ma, Y. Wang, Res. Chem. Intermed. **42**, 481 (2016)
29. Q.D. Qin, Y.H. Liu, X.C. Li, T. Sun, Y. Xu, RSC Adv. **8**, 1071 (2018)
30. T. Zhang, H.B. Zhu, J.P. Croue, Environ. Sci. Technol. **47**, 2784 (2013)
31. M.T. Qiao, X.F. Lei, Y. Ma, L.D. Tian, K.H. Su, Q.Y. Zhang, Chem. Eng. J. **304**, 552 (2016)
32. Y.B. Ding, L.H. Zhu, N. Wang, H.Q. Tang, Appl. Catal. B Environ. **129**, 153 (2013)
33. Y. Feng, D.L. Wu, Y. Deng, T. Zhang, K.M. Shih, Environ. Sci. Technol. **50**, 3119 (2016)
34. J.C. Yan, M. Lei, L.H. Zhu, M.N. Anjum, J. Zou, H.Q. Tang, J. Hazard. Mater. **186**, 1398 (2011)
35. D.H. Ding, C. Liu, Y.F. Ji, Q. Yang, L.L. Chen, C.L. Jiang, T.M. Cai, Chem. Eng. J. **308**, 330 (2017)
36. S.R. Kanel, B. Manning, L. Charlet, H. Choi, Environ. Sci. Technol. **39**, 1291 (2005)
37. Y. Lei, C.S. Chen, Y.J. Tu, Y.H. Huang, H. Zhang, Environ. Sci. Technol. **49**, 6838 (2015)
38. I. Hussain, Y.Q. Zhang, S.B. Huang, X.Z. Du, Chem. Eng. J. **203**, 269 (2012)
39. M.H. Nie, C.X. Yan, M. Li, X.N. Wang, W.L. Bi, W.B. Dong, Chem. Eng. J. **279**, 507 (2015)
40. G.P. Anipsitakis, D.D. Dionysiou, Environ. Sci. Technol. **38**, 3705 (2004)
41. G.S. Timmins, K.J. Liu, E.J.H. Bechara, Y. Kotake, H.M. Swartz, Free Radic. Biol. Med. **27**, 329 (1999)
42. X.G. Duan, H.Q. Sun, J. Kang, Y.X. Wang, S. Indrawirawan, S.B. Wang, ACS Catal. **5**, 4629 (2015)
43. S. Luo, Z.S. Wei, D.D. Dionysiou, R. Spinney, W.P. Hu, L.Y. Chai, Z.H. Yang, T.T. Ye, R.Y. Xiao, Chem. Eng. J. **327**, 1056 (2017)
44. N. Nagar, V. Devra, J. Environ. Chem. Eng. **5**, 5793 (2017)
45. X.Y. Chen, J.W. Chen, X.L. Qiao, D.G. Wang, X.Y. Cai, Appl. Catal. B Environ. **80**, 116 (2008)